Applied Catalysis B: Environmental 204 (2017) 515–524

Contents lists available at ScienceDirect

Applied Catalysis B: Environmental

journal homepage: www.elsevier.com/locate/apcatb

Effect of polyaromatic tars on the activity for methane steam reforming of nickel particles embedded in silicalite-1

D. Laprune, C. Theodoridi, A. Tuel, D. Farrusseng, F.C. Meunier*

Institut de Recherches sur la Catalyse et l'Environnement de Lyon, IRCELYON, Université Lyon 1, CNRS. 2, Av. Albert Einstein, F-69626 Villeurbanne, France

ARTICLE INFO

Article history:
Received 17 October 2016
Received in revised form
24 November 2016
Accepted 1 December 2016
Available online 5 December 2016

Keywords:
Methane steam reforming
Nickel
Rhodium
Tar

ABSTRACT

The steam reforming of methane was studied over Rh and Ni-based catalysts exposed to naphthalene, which was used as a representative of polyaromatic tars found in biomass-derived biogas. In particular, two Ni-based samples in which part of the metal was encapsulated within silicalite-1 nanoboxes were tested. The reforming reaction was carried at 700, 800 and 900 °C using a model feed and high space velocities to limit methane full conversion and better evidence any deactivation. A strong decrease of methane conversion was observed in the presence of 1400 ppm of naphthalene, stressing the marked deleterious effect of this molecule in the present conditions. The effect of naphthalene was partly reversible, especially at higher temperatures. The silicalite-1 membrane could not prevent the deactivation of embedded nickel particles, probably because naphthalene (kinetic diameter = 0.62 nm) could diffuse throughout the MFI-type (pore diameter ca. 0.56 nm) porous layer at the high reaction temperatures used. The effect of 5 ppm of the bulkier pyrene (kinetic diameter = 0.74 nm) was investigated at 700 °C and also led to a rapid deactivation of the Ni@silicalite-1, likely because pyrene was cracked into naphthalene, which could then enter the silicalite-1 nanoboxes. The poisoning effect of toluene on the Ni-based catalysts was minor in comparison to that induced by the polyaromatics. A marked sintering of the embedded Ni was also observed.

1. Introduction

Syngas, a mixture of carbon oxides and dihydrogen, can be obtained from the steam reforming of fossil fuels [1–5] and the gasification of biomasses or carbon-containing wastes [6,7]. The gas obtained from biomass gasification contains significant concentrations of light hydrocarbons and tars that should be preferably reformed to increase syngas yield [8,9].

Tars, a mixture of condensable organic compounds such as mono- and polyaromatics, are well known coke precursors that can lead to the deactivation of reforming catalysts. The propensity for coke formation from tars will depend on the catalyst formulation and reaction conditions such as reaction temperature and steam/carbon (S/C) ratio. Di Carlo et al. reported no deactivation at 800 °C of $Ni/Ca_{12}Al_{24}O_{33}$ used for the steam reforming of tars derived from hazelnut shells gasification [10]. Sato and Fujimoto also reported stable naphthalene conversions at 825 °C over a WO_3-promoted Ni/MgO—CaO catalyst, even in the presence of H_2S [11].

The impact of tars on the reforming of methane is less documented. Dagle et al. recently showed that the presence of benzene and naphthalene led to marked deactivations of methane conversion due to coking over Ni, Rh and Ir-based catalysts [12]. The coking was alleviated by using higher reaction temperatures and by the presence of a noble metal.

The support has no direct role on the methane reforming, except for the dispersion and stabilization of metal particles [13]. High metal dispersion is important to achieve high specific activities. The reaction is thought to be structure-sensitive, low coordination metal sites exhibiting somewhat higher turn-over frequencies [14–16]. Ni is intrinsically less active than noble metals [13,16], but has a lower cost. The use of $MgAl_2O_4$ spinel as a support is often favored over that of alumina, especially because Ni can form a spinel phase with the latter that is difficult to reduce to metallic Ni [17].

Extensive carbon deposition can yet occur on Ni-based catalysts that can be of several types, i.e. pyrolitic, encapsulating and whiskers [18,19]. Encapsulating carbon (also referred to as "gum") is formed during reforming of feeds containing aromatic compounds. The formation of whiskers, which have high mechanical strength, can lead to catalyst particle breaking up and a large pressure drop increase in the reactor. The deposition of carbon is overall

* Corresponding author.
E-mail address: fcm@ircelyon.univ-lyon1.fr (F.C. Meunier).

http://dx.doi.org/10.1016/j.apcatb.2016.12.004
0926-3373/

a complex interplay between methane/hydrocarbon decomposition and carbon gasification [20].

In the present work, two commercial catalysts based on Rh and Ni were studied, as well as two Ni-based samples in which part of the metal was encapsulated in silicalite-1 (MFI structure) nanoboxes. The effect of naphthalene on methane conversion was investigated at 700, 800 and 900 °C and, importantly, high space velocities to limit the full conversion of methane and better assess deactivation. Additional experiments were also performed using toluene and pyrene to unravel the main origin of the deactivation.

Our investigation focused on naphthalene because this molecule is one of the most difficult tar representatives to steam reform [21,22] and one of the most abundant among the polyaromatics formed during low-temperature gasification [23] and fast-pyrolysis [24] of woody biomasses. Naphthalene is also the smallest polyaromatic available and thus any catalyst that would display a size-selective resistance with respect to this molecule should also do so for the other larger compounds.

Naphthalene has a kinetic diameter of 0.62 nm, which is larger than the pore diameter of MFI zeolites (ca. 0.56 nm). Millini et al. reported that diffusion of naphthalene in the medium pore-size zeolite of the MFI-type was difficult, with energy barriers of around 114 kJ/mol [25]. In contrast, the transport of H_2O, CO_2, CO, H_2 and CH_4 (and many other small hydrocarbons) through the MFI zeolite layer is markedly faster. It is therefore possible that the slow transport of naphthalene though MFI-type pores could protect the metal particles encapsulated therein from coking, through the interplay of coke formation and gasification/reforming. These materials would thus exhibit size selective properties, being able to steam reform small hydrocarbons, while being resistant against coking due to large polyaromatics.

We reported earlier on the total size exclusion of mesitylene (kinetic diameter = 0.87 nm) from MFI-type silicalite-1 hollow nanocrystals [26,27]. In addition, we also have reported that these nanoboxes act as nanoreactors [28,29] in which the nanoparticles are encapsulated and protected from sintering by coalescence [30]. The activity and durability of Ni particles embedded in similar silicalite-1 nanoboxes during steam methane reforming catalyst will be of particular interest here, since the effect of operating at temperatures as high as 900 °C has not yet been reported. The synthesis and characterization of the Ni@silicalite-1 samples used here are described in details elsewhere [31] and are only briefly recalled here.

2. Experimental section

2.1. Catalyst synthesis

Silicalite-1 was prepared using tetraethylorthosilicate (TEOS, Aldrich, 98%) and 1 M TPAOH solutions obtained from aqueous TPABr by exchange with Ag_2O. The gel of composition SiO_2-0·4TPAOH-35H_2O was stirred at room temperature overnight to fully hydrolyze the TEOS, then transferred into a Teflon-lined autoclave and heated at 170 °C under static conditions for 3 days. The autoclave was then cooled to room temperature and the solid was centrifuged, washed with water until pH = 7 and dried overnight at 90 °C. Finally, the resulting solid was calcined for 12 h at 525 °C in air yielding silicalite-1 crystals of approximately 200 × 150 × 140 nm in size.

Ni@silicalite-1 materials were synthesized following the previously described generic method for the encapsulation of transition metal nanoparticles in hollow silicalite-1 single crystals [26,27,30,32,33–35]. In brief, 5 wt.%Ni@silicalite-1 catalyst was prepared by incipient wetness impregnation: 2 mL of $Ni(NO_3)_2$-6(H_2O) (99.999%, Sigma-Aldrich) aqueous solution with a

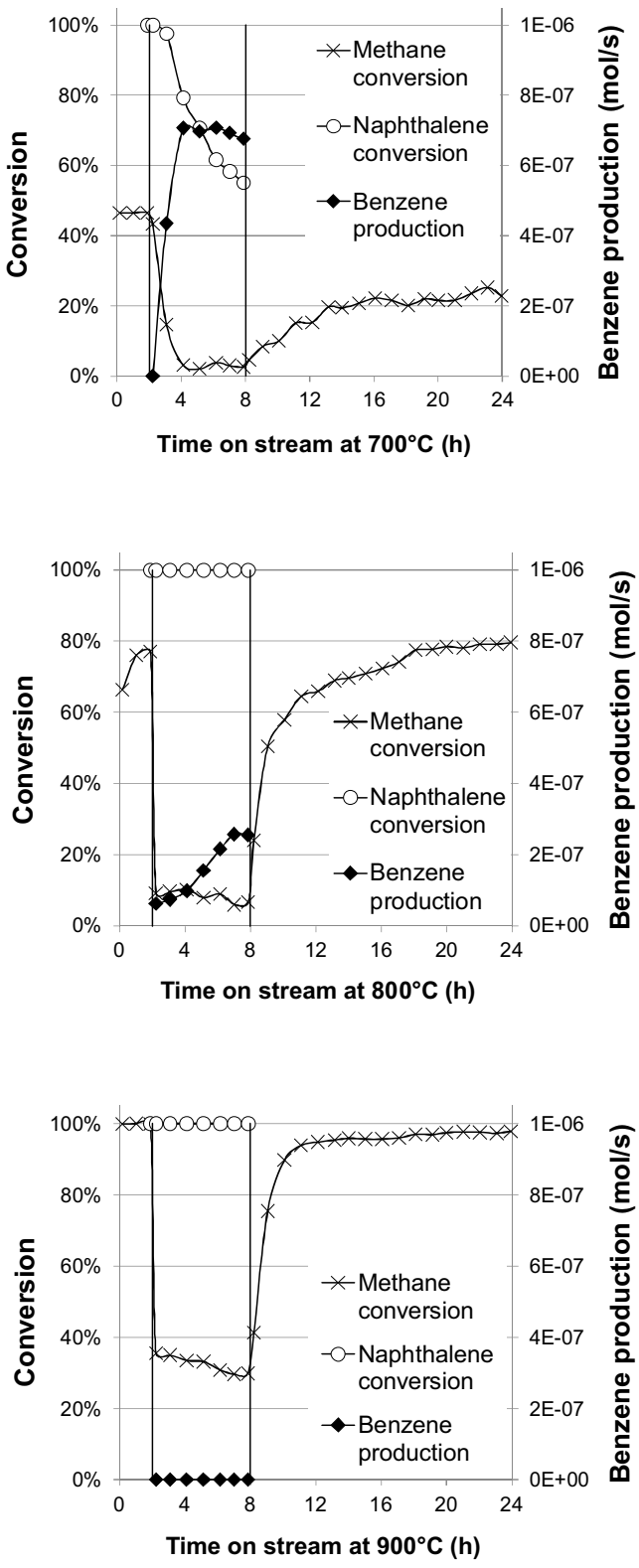

Fig. 1. Methane and naphthalene conversions and benzene production measured over time on stream at 700, 800 and 900 °C over the Rh-based commercial catalyst. 1400 ppm of naphthalene were introduced in the feed between 2 h and up to 8 h.

Table 1
Composition and textural properties of the catalysts reduced at 750 °C. Textural data are based on the calculations of the corresponding d_{SW} [b] (respectively H_2 chemisorption measurements) in case of the zeolite-based samples (resp. commercial samples).

Catalyst	Support	S_{BET} ($m^2\ g^{-1}$)	Metal loading (wt.%)	Mean metal particle diameter (nm)	Metal dispersion (%)
Commercial Rh	γ-Al_2O_3 [a]	150	0.8	1.7 ± 0.2	63 ± 1
Commercial Ni	$CaAl_2O_3$ [a]	14	11.4	44 ± 1	2.3 ± 0.1
5%Ni@sil-1	hollow silicalite-1	338	6.2	8 ± 3 [b]	16 ± 7
CitAc Ni@sil-1	hollow silicalite-1	272	1.5	4.6 ± 1 [b]	26 ± 7

[a] Based on XRD analyses.
[b] Surface-weighted mean diameter (incertitude based on distribution standard deviation – 500 particles counted).

concentration of 426 mmol/L was added to 1 g of silicalite-1, which had been outgassed at 300 °C overnight. The mixture was stirred at 50 °C until complete evaporation of water to obtain the $Ni(NO_3)_2$-silicalite-1. The hollow structure was obtained by treating 1 g of this material in a TPAOH aqueous solution (7.5 mL; 0.55 M) in a Teflon-lined autoclave at 170 °C under rotating conditions for 24 h. The solution was then cooled down, washed with water until pH = 7, dried overnight at 90 °C and calcined at 450 °C for 6 h to obtain the NiO@silicalite-1. Finally the solid was reduced at 750 °C under H_2 for 3 h with a heating rate of 2.5 °C/min to yield the nominal loading 5%Ni@sil-1. The actual metal loading was 6.2 wt.% (Table 1). A Ni-free hollow silicalite-1 sample was prepared according to the same procedure without any Ni impregnation.

A citric acid post-treatment was used to remove external Ni particles [31]. 500 mg of NiO@silicalite-1 was added to 50 mL of citric acid (≥ 99.0%, Sigma-Aldrich) aqueous solution with a concentration of 0.5 mol/L and the mixture was stirred vigorously at 80 °C for 2 h. The solution was then centrifuged and washed with water until pH = 7 and dried overnight at 90 °C. Finally the solid was also reduced at 750 °C under H_2 for 3 h to yield a sample referred to as CitAc Ni@sil-1.

In addition to the silicalite-1-based materials, a commercial Rh-based catalyst (1%Rh/Al_2O_3, Alfa Aesar, ref. 11769) and a commercial Ni-based catalyst (HiFUEL R110, Alfa Aesar, ref. 45465) were used as reference catalysts.

2.2. Catalyst characterization

Powder X-ray diffraction patterns (XRD) were recorded to assess the crystallinity of the samples. Diffractogrammes were collected between 4 and 90° (2Θ) with steps of 0.02° and 1 s per step with a Bruker D5005 diffractometer using CuKα radiation at λ = 1.5418 Å. Relative crystallinity of silicalite-1-based catalysts was calculated following a standard method [36]described as follow:

$$\text{Lossincrystallinity} = (\%\text{Crystallinity}_{\text{fresh}} - \%\text{Crystallinity}_{\text{post-mortem}})/\%\text{Crystallinity}_{\text{fresh}}$$

$$\text{where\%}\quad \text{Crystallinity} = (\text{Area}_{2\theta = 22.5\text{–}25^\circ}/\text{Area}_{\text{reference}2\theta = 22.5\text{–}25^\circ}) \times 100$$

and where $\text{Area}_{\text{reference}2\theta = 22.5-25^\circ}$ was measured on a fully crystalline plain silicalite-1 sample used as a reference. The size of the crystalline domains of Ni particles was calculated using the Scherrer formula based on peak broadening of the two most intense peaks of metal Ni (44° and 51°, JCPDS: 04-0850).

Elemental analysis of the fresh catalysts was performed using an ICP-OES ACTIVA from HORIBA Jobin Yvon equipped with a CCD detector for the determination of metallic loadings. Nitrogen adsorption isotherms were measured at 77 K on a Belsorp-mini from BEL-Japan and a Micromeritics 3Flex. Samples were outgassed under vacuum at 150 °C for 4 h.

TEM pictures were obtained using a Jeol 2010 LaB6 microscope operating at 200 kV. Particle size distributions (PSDs) of zeolite-based materials were obtained by counting 500 particles using Image J software [37]. Surface-weighted mean diameters $d_{SW} = \Sigma n_i d_i^2 / \Sigma n_i d_i^3$ were calculated from the PSDs, where n_i is the number of particles counted with a diameter d_i. Metal dispersions were deduced from the corresponding d_{SW} considering a cuboctahedral model and a calculation method described by Van Hardeveld and Hartog [38]. EDX measurements were performed using an EDX Link ISIS analyzer from Oxford Instruments to identify the elements present in the samples.

Metal surface areas were also measured by hydrogen chemisorption at 35 °C using a Micromeritics ASAP 2010. The sample holder was loaded with 0.5 g of catalyst and prior to the measurement the catalyst sample was reduced in situ in flowing hydrogen at 700 °C for 2 h. After reduction, the sample was evacuated for 2 h at 350 °C before cooling down to 35 °C. Two successive adsorption isotherms, separated by a second evacuation of 1 h at 35 °C, were then measured, according to the method described by Iglesia and co-workers [39]. The amount of hydrogen chemisorbed was obtained by correcting the total hydrogen uptake (1st isotherm) with that of weakly adsorbed H_2 (2nd isotherm). Nickel (respectively rhodium) surface areas were calculated assuming a $H/Ni_{surface} = 1$ (resp. $H/Rh_{surface} = 2$) ratio [40,41] and a Ni (resp. Rh) atom area of 6.51×10^{-20} m^2 (resp. 7.58×10^{-20} m^2) [42]. Specific surfaces (S_M) were converted to mean particle diameters (d_M) assuming a spherical particle shape, resulting in:

$$d_M(\text{Å}) = 60000/(\rho(\text{g cm}^{-3}) \times S_M(\text{m}^2\ \text{g}^{-1}))$$

where ρ is the metal mass density. Metal dispersion (D_M) values were deduced considering:

$$D_M(\%) = 6\,x((v_M(\text{Å}^3)/a_M(\text{Å}^2))/d_M(\text{Å})) \times 100$$

where a_M and v_M are respectively the area occupied by a surface atom and the volume occupied by a bulk atom.

The amount of carbon deposited on spent catalysts was measured by thermogravimetric analysis (TGA) on a Mettler Toledo TGA/DSC1 thermal analyzer. About 4 mg of spent catalyst was used in each TGA experiment during which the sample was heated in air flown at 50 mL/min up to 900 °C at a heating rate of 5 °C/min.

2.3. Steam reforming tests

The steam reforming experiments were performed on a lab-scale system (Scheme 1). The tests were carried out in a fixed-bed continuous-flow reactor consisting of a quartz tube (length 300 mm, 4 mm ID, 6 mm OD) containing 10 mg (unless otherwise stated) of non-diluted catalyst held between plugs of quartz wool. The commercial Rh-based catalyst powder was tested without any pre-shaping. The commercial Ni-based pellets and "ship-in-a-bottle" materials (5%Ni@sil-1 and CitAc Ni@sil-1) were crushed and sieved to obtain particle sizes ranging from 100 to 200 μm. Prior to testing, catalysts were reduced in situ at 700 °C (heating rate of 400 °C/h) for 2 h under a flow of 200 mL/min of 20 vol.% H_2/Ar mixture. The typical bed height varied between 0.5 and 3 mm, meaning that the reactor could not be considered in a plug-flow regime.

A model gas composition was used (Table 2) that was similar to that of typical reformate compositions [43]. Brooks Instrument mass flow controllers (MFC) were used to control gas flow rates of H_2, CH_4, CO, CO_2, N_2 and Ar. The overall system pressure was set

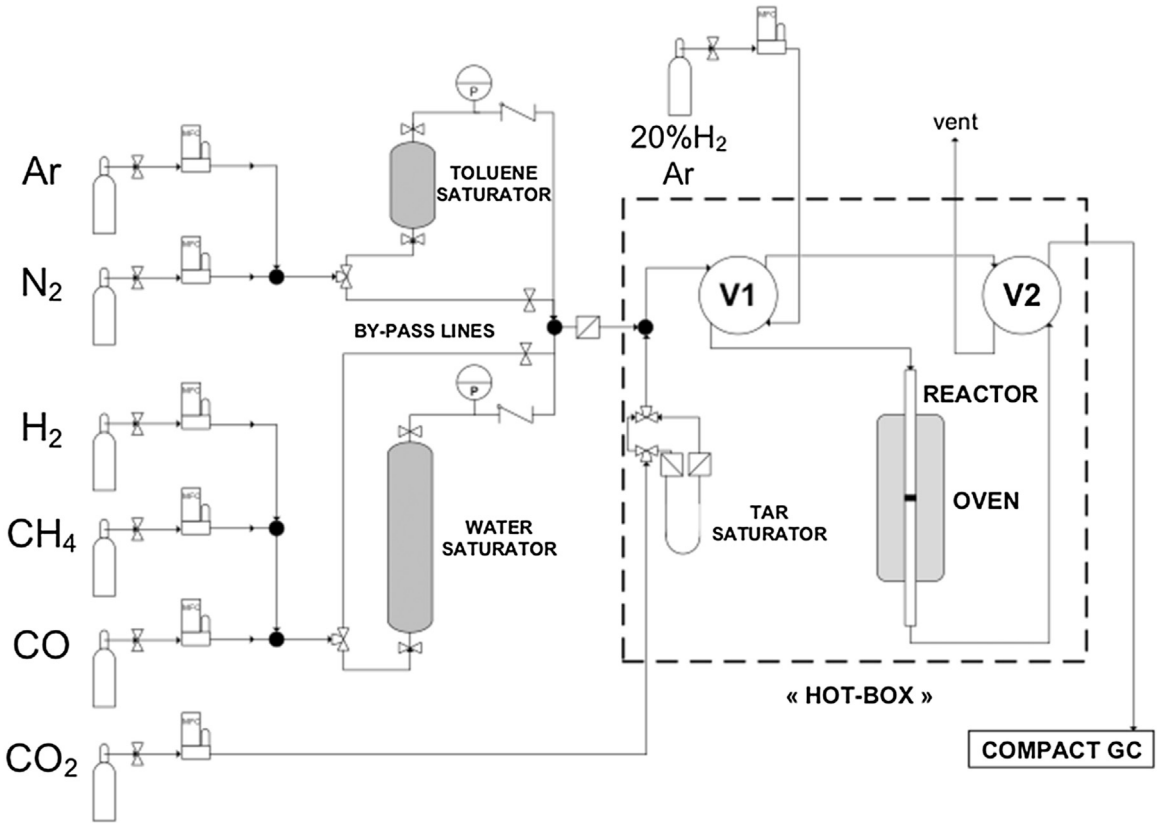

Scheme 1. Schematic layout of the experimental setup.

Table 2
Feed gas composition for catalytic reforming tests.

Compound	CO	H_2	CO_2	H_2O	CH_4	N_2	Ar	Tar model compound, if any
(vol.%)	20	16	10	39	9	2	4	Naphthalene: 1400 ppm Pyrene: 5 ppm Toluene: 1%

at P_{total} = 2.2 bar using a needle valve located downstream the on-line analyzer. A pressure sensor was placed upstream of the reactor to check for a possible pressure increase due to bed blocking. Solid naphthalene (or pyrene) was placed in a U-shaped ¼" stainless steel tube saturator in the hotbox set at 107 °C and water was placed in a 500 mL cylindrical saturator set at 99 °C. Toluene was placed in a 150 mL cylindrical saturator set at 82 °C. Carrier gas flow rates were set to obtain the desired flow rates of steam and the tar model used (i.e. toluene, naphthalene or pyrene). The catalytic bed was located in the isothermal region of a tube furnace and the temperature was monitored by a thermocouple placed inside the furnace. The catalyst was tested sequentially at 700, 800 and 900 °C, dwelling 24 h at each temperature. At each temperature, naphthalene (or pyrene) was only introduced in the feed between t = 2 h and up to t = 8 h. The reversibility of the deactivation was then studied by maintaining the catalyst under a naphthalene-free feed for up to 16 h.

Online analysis of the reactor effluent was performed with a Compact GC (CGC) from Global Analyzer Solutions. The analyzer was equipped with two columns coupled with TCD and FID analyzers enabling the quantification of permanent gases (N_2, H_2, CO, CO_2 and CH_4) and hydrocarbons (CH_4 and heavier), respectively. The N_2 signal was used as an internal standard for the TCD channel to convert the other surface areas into molar flows. Similarly, the CH_4 signal was used as an internal standard for the FID channel (the CH_4 molar flow rate being itself determined from the TCD channel). H_2O quantification was not performed. Quantitative analyses of permanent gases were performed by calibrating the CGC using different partial pressures of compounds diluted in N_2. On the FID channel, hydrocarbons of interest were quantified by determining their response factor relative to CH_4.

The total gas flow rate of reactants was 125 mL min^{-1}. The corresponding WHSV was 689 h^{-1} (the GHSV was 750 000 h^{-1}, assuming catalyst density to be unity). This high WHSV value was selected to obtain an accelerated ageing in terms of tar exposure on a reasonable timescale. Furthermore, these conditions prevented total conversion of hydrocarbons, providing insights in terms of activity and stability of the different catalysts. Reactor modeling using the Eurokin Gas-Solid fixed bed reactor modeler [44] indicated the presence of a significant radial heat transport limitation resulting in a cold spot of up to 45 °C when the reactor was operated at 900 °C.

3. Results and discussion

3.1. Sample characterizations

Sample characterizations before catalytic tests are detailed elsewhere [31]. The Ni loading measured by ICP on the 5%Ni@sil-1 was

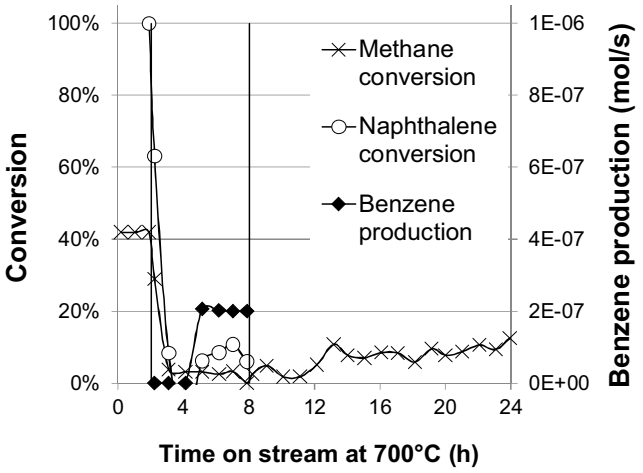

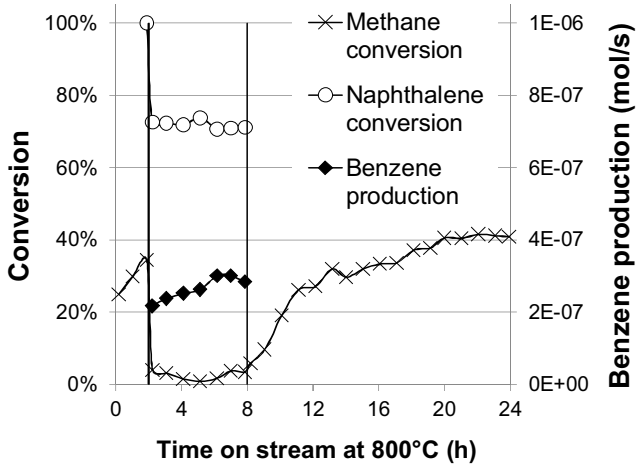

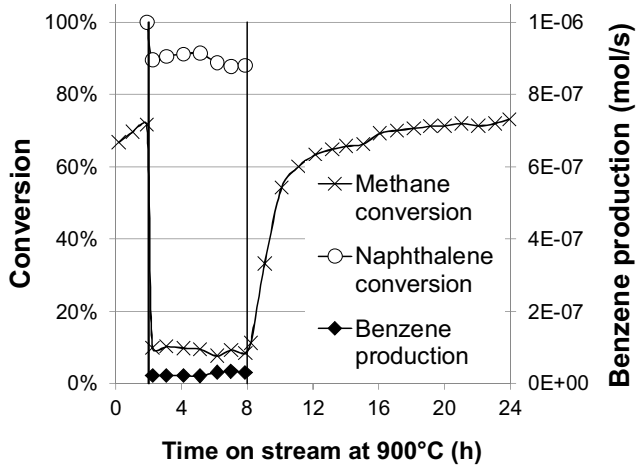

Fig. 2. Methane and naphthalene conversions and benzene production measured over time on stream at 700, 800 and 900 °C over a Ni-based commercial catalyst. 1400 ppm of naphthalene were introduced in the feed between 2 h and up to 8 h.

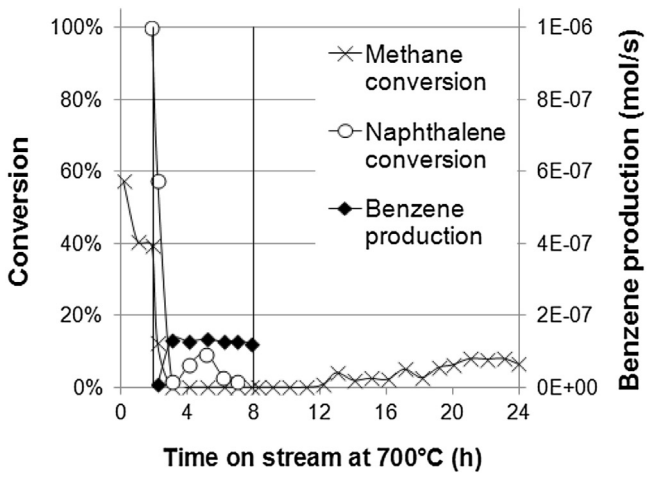

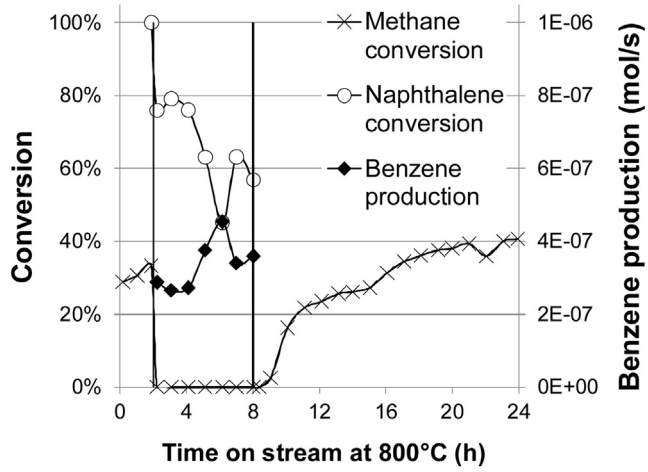

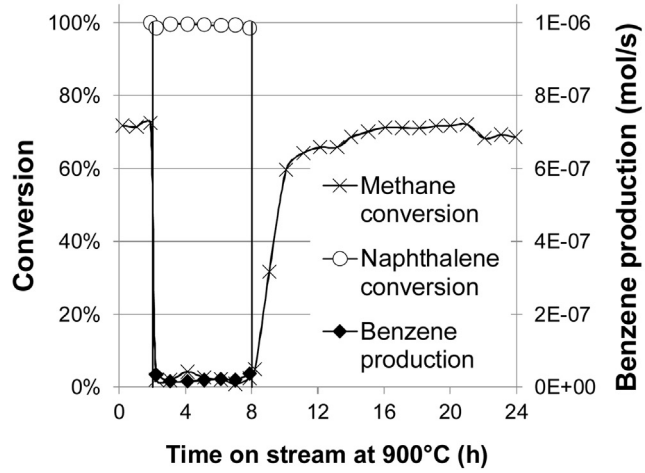

Fig. 3. Methane and naphthalene conversions and benzene production measured over time on stream at 700, 800 and 900 °C over 5 wt.% Ni@sil-1 catalyst. 1400 ppm of naphthalene were introduced in the feed between 2 h and up to 8 h.

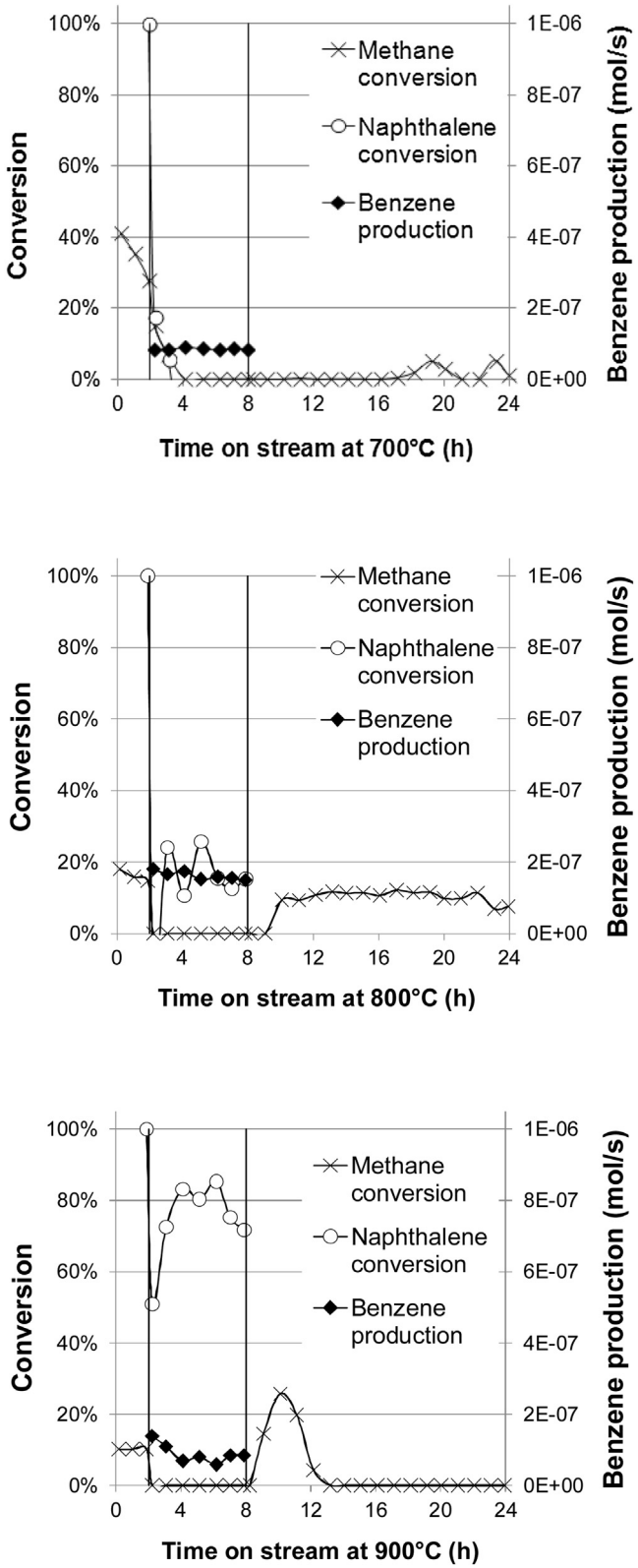

Fig. 4. Methane and naphthalene conversions and benzene production measured over time on stream at 700, 800 and 900 °C over CitAc Ni@sil-1. 1400 ppm of naphthalene were introduced in the feed between 2 h and up to 8 h.

6.2 wt.%, close to the nominal value (Table 1). The loss of Ni due to the citric acid treatment was extensive, resulting in the Ni loading dropping from 6.2 down to ca. 1.5 wt.%. The average particle sizes were below 10 nm for both nanobox-based samples. The citric acid treatment also led to a decreased average particle size, which was due to the removal of more than 90% of larger Ni particles located outside the nanoboxes [31].

3.2. Steam reforming activity

The effect of the addition of 1400 ppm of naphthalene on the activity of the various catalysts was determined at 700, 800 and 900 °C in succession during the same experiment using the same batch (Figs. 1–4). This implies that the catalyst may have partly deactivated at the lower temperatures before being used at the higher ones. At each temperature and for all the catalysts, the introduction of naphthalene led to a sharp and almost total loss of the conversion of methane. The poisoning effect of this hydrocarbon appeared to be only partly and slowly reversible at 700 °C over the commercial Ni and Rh catalysts (Figs. 1 and 2). Yet, methane conversion was fully and readily recovered at 800 and 900 °C over these two commercial samples (Figs. 1 and 2) and the 5 wt.% Ni@silicalite-1 (Fig. 3). It should be noted that benzene was formed as a decomposition product of naphthalene.

The 5 wt.% Ni@sil-1 catalyst and especially the citric acid-treated CitAc 5%Ni@sil-1 sample appeared to deactivate even before the introduction of naphthalene (Fig. 4). This initial deactivation could be due to both Ni sintering (enhanced by the presence of steam [18] and the poor anchoring properties of silicalite-1) and coke formation. These nanobox-based catalysts showed a strong deactivation in the presence of naphthalene at all temperatures (Fig. 4). This was a disappointing result particularly for the CitAc 5%Ni@sil-1 because most of the Ni particles were initially embedded inside the silicalite-1 nanoboxes in this sample [31] and were expected to show a better resistance against the bulky naphthalene molecules.

The activity at 900 °C showed a peculiar behavior, with a transient activity spike followed by total deactivation (Fig. 4), contrary to the case of the sample not-treated by citric acid (Fig. 3). A close inspection of these two samples post-reaction by TEM indicated that the structure of nanoboxes of the citric acid-treated sample had totally collapsed (Fig. 5, bottom), contrary to the case of the 5%Ni@sil-1 sample (Fig. 5, top). In addition, the size of the Ni particles had increased markedly for both samples, from below 10 nm (Table 1) up to ca. 35 nm (Fig. 6, Table 3).

Comparing the average Ni crystallite sizes before and after reaction (Table 1 and Fig. 6), the CitAc 5%Ni@sil-1 sample was even more prone to particle agglomeration (8-fold increase of the average particle diameter) than the non-treated sample (4-fold increase). This observation underlines the ability of the hollow zeolite shell to limit Ni nanoparticles sintering, at least until the complete breakup of the nanobox structure occurred.

An XRD analysis (Fig. 7, Table 3) revealed that both samples exhibited a loss of crystallinity of the silicalite-1 phase after reaction. The formation of cristobalite was also apparent in the case of the CitAc Ni@sil-1, stressing the lower thermal stability of the citric-acid-treated sample [45]. The Ni crystallite sizes (determined through the Scherrer equation) dramatically increased to about 36 nm following reaction (Table 3), while those were lower than 10 nm before reaction. It should be noted that the Ni particle sizes determined by TEM and XRD are fully consistent (Table 3).

The formation of carbonaceous species, mostly present as graphitic whiskers, was also detected from TEM observations on both aged silicalite-1-based samples (Fig. 5, right). Some carbon whiskers ending with Ni particles were also visible. The results of thermogravimetric analyses for the quantification of this residual coke are presented in Table 3. The recorded mass loss in the tem-

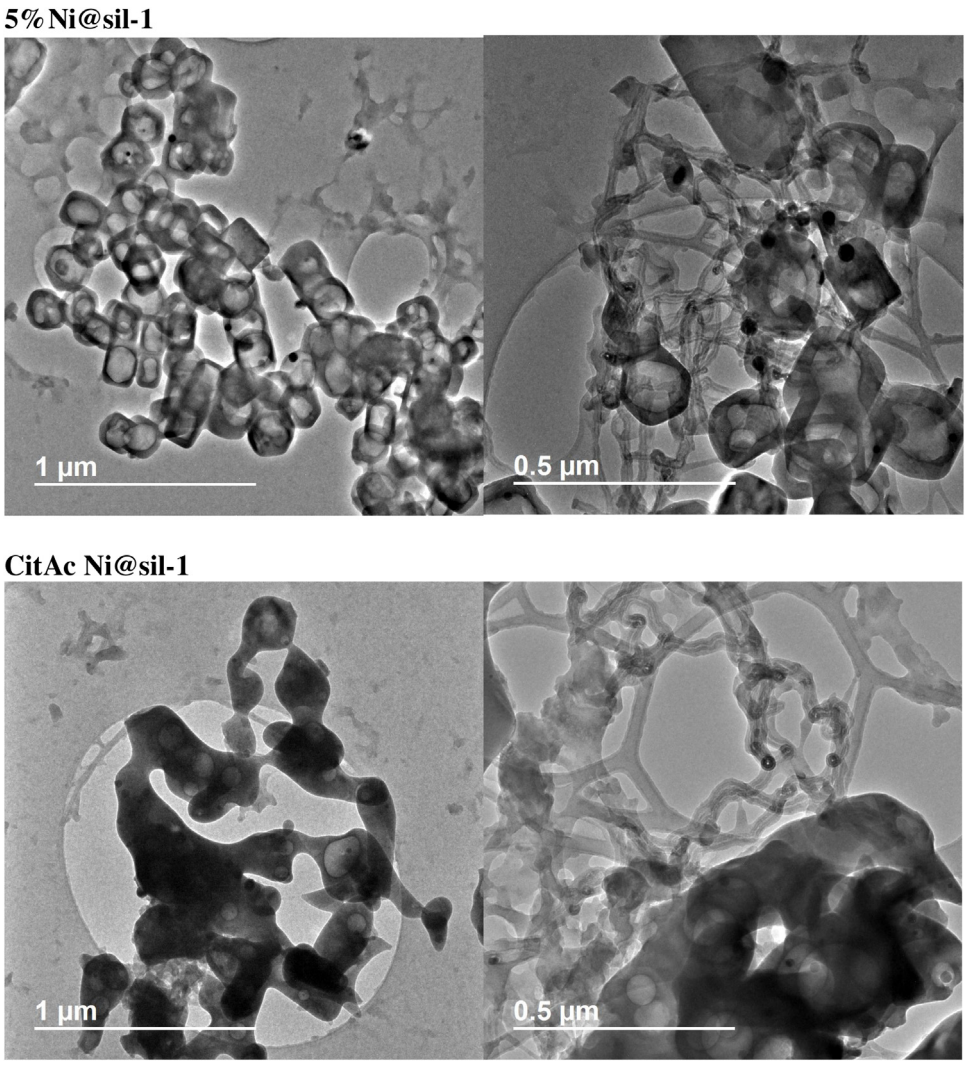

Fig. 5. TEM images of post-reaction 5%Ni@sil-1 (top) and CitAc Ni@sil-1 (bottom) using magnification of ×5000 (left) and x10000 (right).

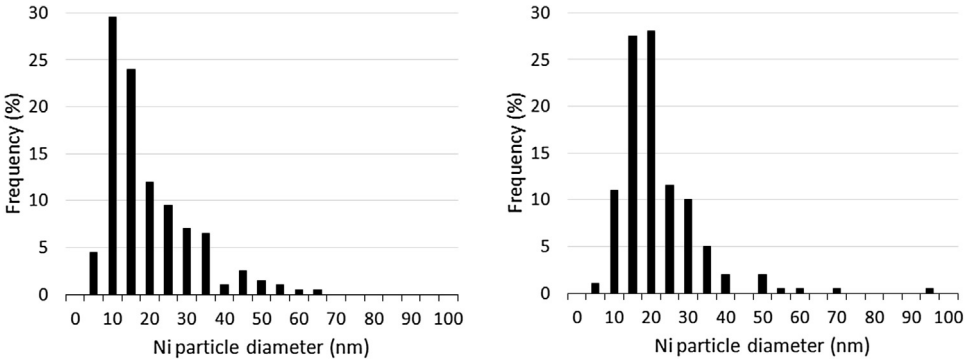

Fig. 6. Post-reaction particule size distributions of 5%Ni@sil-1 (left) and CitAc Ni@sil-1 (right). Measurements based on 200 particles.

Table 3
Calculation of the loss in silicalite-1 cristallinity (%) and of the Ni crystallite size (nm) using both the Scherrer equation (XRD) and the surface-weighted mean diameters (TEM) for post-mortem analysis of the 5%Ni@sil-1 and CitAc Ni@sil-1. The mass loss obtained by thermogravimetric analyses is also given.

	% Loss in silicalite-1 crystallinity	Initial Ni crystallite size (nm)	Ni crystallite size post-reaction		Dispersion Post-reaction	TGA mass loss ($g\,g^{-1}_{cat}$)
			XRD (nm)	TEM (nm)		
5%Ni@sil-1	44	8	32	35	3.7%	1.7×10^{-3}
CitAc Ni@sil-1	90	4.6	35	37	3.5%	1.1×10^{-2}

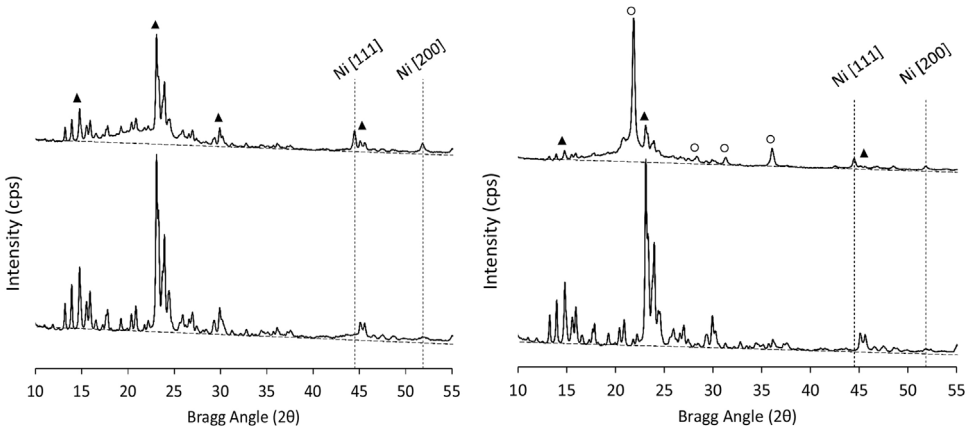

Fig. 7. XRD analysis of fresh (bottom diffractogram) and post-reaction (top diffractogram) 5%Ni@sil-1 (left) and CitAc Ni@sil-1 (right). Post-reaction diffractograms indicate an increase of the baseline in the range 2θ = 12–40° corresponding to sample amorphisation. (▲): silicalite-1 (JCPDS: 48-0136). (O): Cristobalite (JCPDS: 39-1425). No indication of carbon graphite formation is observed (characteristic peak at 2θ = 28°).

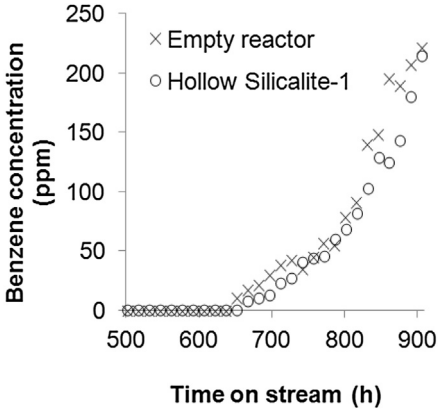

Fig. 8. Benzene concentration measured in the reactor effluent while reforming methane in presence of naphtalene on an empty reactor (x) and one filled with Ni-free hollow silicalite-1 (o).

perature range 550–650 °C was attributed to the combustion of graphitic carbon only, since identical analyses on the corresponding fresh samples exhibited no mass loss over the same range. These results are consistent with literature data related to whisker gasification on similar catalysts [46,47]

The observed major sintering of Ni particles could yet not be the cause of the reversible deactivations observed in the presence of naphthalene over the 5%Ni@sil-1 (Fig. 3), since Ni redispersion upon removing naphthalene is not expected. Ni sintering over the 5%Ni@sil-1 is likely to have occurred in the very first instants following exposure to the steam-containing feed at 700 °C, as suggested by the initial decay of methane conversion observed at 700 °C (Fig. 3), and also during the subsequent temperature increases to 800 and 900 °C. The reversible deactivation likely arose from carbon deposition, as suggested by the TGA analyses (Table 3) and TEM pictures (Fig. 5, right)

Complementary methane steam reforming experiments were carried out to unravel the nature, i.e. mono or polyaromatic, of the molecule responsible for the coking taking place in the presence of naphthalene, as benzene was observed in all experiments (Figs. 1–4). It must be stressed that benzene was formed from naphthalene even in the absence of any catalyst (and over a Ni-free silicalite-1 sample) above 650 °C (Fig. 8). This fact is important because it shows that heavy aromatics will thermally crack into monoaromatics at the typical reaction temperatures needed to steam reform methane. Monoaromatics are expected to readily diffuse throughout silicalite-1 membranes [26,27,30]. It was therefore necessary to ascertain the role of monoaromatics on the deactivation under our conditions.

The use of toluene was preferred to that of benzene for the sake of convenience, especially since the propensity for coking of these two molecules is expected to be similar. The presence of 1% of toluene induced a significant deactivation of the Rh-based commercial catalyst at 800 and 700 °C (Fig. 9). Any potential deactivation at 900 °C could not be ascertained because methane conversion was too close to 100%. The deactivation obtained using a large concentration of toluene (1%) appeared yet more limited than that observed under 1400 ppm of naphthalene (Fig. 3) over (10 mg) of the same sample.

A bed blockage was observed in the case of the commercial Ni-based catalysts at 700 °C after ca. 18 h on stream (Fig. 10). This is consistent with the extensive formation of carbon whiskers (as observed in Fig. 5, right) on Ni particles under reforming conditions, especially at low temperatures. Formation of whiskers, leading to Ni particles being detached from the support, yields hardly any conversion loss until the catalyst bed becomes fully blocked [48].

In the case of Ni, the poisoning effect of toluene (Fig. 10) was almost negligible as compared to that of naphthalene (Fig. 2). It can be concluded that monoaromatics are unlikely to be responsible for the strong deactivation of Ni-based samples induced by naphthalene. Therefore, we propose that naphthalene itself directly poisoned the Ni particles located inside the silicalite-1 nanoboxes through the formation of encapsulating coke and whiskers [19,48] process which appeared slowly reversible over most samples at the higher temperatures (Figs. 1–4).

The CitAc Ni@sil-1 sample was the most deactivated by naphthalene (Fig. 4) and its nanobox structure eventually almost totally collapsed (Fig. 5 and Table 3). This is in contrast to the case of the 5%Ni@sil-1, for which the shape of the nanoboxes was preserved (Fig. 5) as well as a much higher degree of crystallinity (Table 3). One possible explanation for this difference is that most of the nickel was embbeded within the CitAc Ni@sil-1 sample and this is thus where most of the coke formation would have occurred. Since carbon whiskers were also formed (observed by TEM, Fig. 5) and posses high mechanical strength[19] those probably broke up the nanoboxes. In the case of the 5%Ni@sil-1, it is likely that most of the coke formation took place on the Ni that was in most part located outside the nanoboxes. This probably resulted in the blocking of the silicalite-1 pores by encapsulating coke (easily formed from polyaromatics [18]) and thereby limited access to the Ni contained in the hollow core of the nanoboxes and coke formation inthere.

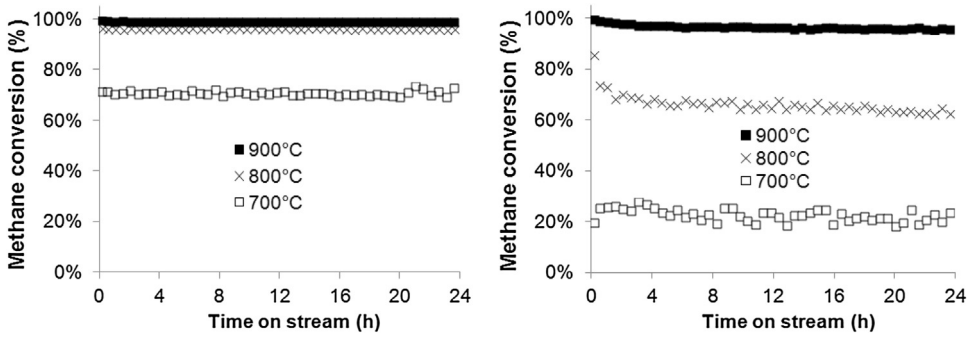

Fig. 9. Methane conversions measured with time on stream at 700, 800 and 900 °C over the Rh-based commercial catalyst in absence (left) and in presence (right) of 1% of toluene. Catalyst mass = 25 mg.

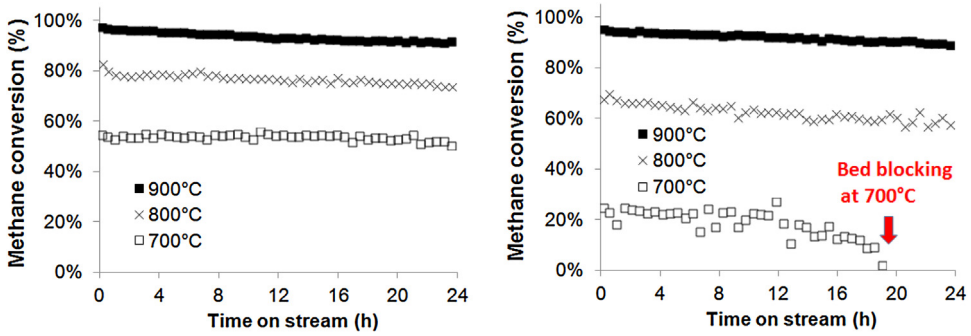

Fig. 10. Methane conversions measured with time on stream at 700, 800 and 900 °C over the Ni-based commercial catalyst in the absence (left) and in presence (right) of 1% of toluene. Catalyst mass = 25 mg.

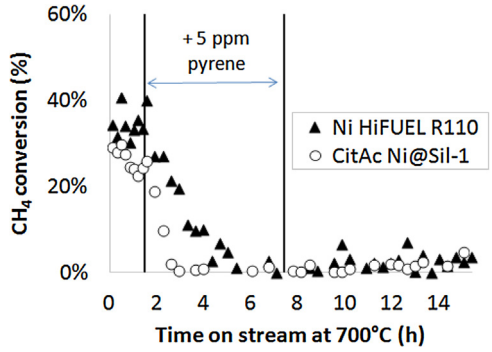

Fig. 11. Methane conversions measured with time on stream at 700 °C over 25 mg of the Ni-based commercial catalyst (Ni HiFUEL 110) and the CitAc Ni@sil-1 sample. 5 ppm of pyrene were introduced over a period of 6 h.

Since naphthalene appeared to be able to cross the silicalite-1 membrane of the CitAc Ni@sil-1, an additional experiment was carried out using a much bulkier polyaromatic, i.e. pyrene (kinetic diameter = 7.24) [49]. A concentration of 5 ppm of pyrene appeared to readily deactivate the commercial Ni-based catalyst (Fig. 11), but also the CitAc Ni@sil-1 sample. Since naphthalene was observed in the reactor effluent, it is proposed that naphthalene or some other cracking product of pyrene could have coked the embedded nickel. The deactivation of the CitAc Ni@sil-1 appeared to be faster than that of the commercial Ni-based catalysts, possibly because of the lower concentration of Ni present on the former.

4. Conclusions

A concentration of 1400 ppm of naphthalene readily and strongly poisoned the steam reforming of methane over Rh and Ni-based catalysts. The use of encapsulated Ni@silicalite-1 samples did not lead to naphthalene-resistant catalysts, most likely because this molecule was able to access the embedded Ni in spite of the silicalite-1 nanobox membrane surrounding the metal particles. The bulkier pyrene, at a concentration of 5 ppm, lead to similar results, as pyrene was shown to partly crack into naphthalene. In contrast, the effect of a monoaromatic such as toluene was almost negligible on the activity of Ni-based samples, apart from possible bed blocking through carbon whisker formation at low temperature (700 °C). The silicalite-1 single hollow nanobox was inefficient in preventing the sintering of Ni particles. This work emphasize the difficulty in obtaining size-selective systems for high temperature applications, since reactant cracking is common and a range of smaller molecules are generated in situ.

Acknowledgments

This work was partly supported by the European Union Seventh Framework Programme FP7-NMP-2013, under Grant Agreement number 604277 (acronym FASTCARD). Prof X. Verykios from Patras University is acknowledged for organizing the exchange of C.T.

References

[1] G. Jones, J. Jakobsen, S. Shim, J. Kleis, M. Andersson, J. Rossmeisl, F. Abildpedersen, T. Bligaard, S. Helveg, B. Hinnemann, J. Catal. 259 (2008) 147.
[2] P. Ferreira-Aparicio, A. Guerrero-Ruiz, I. Rodríguez-Ramos, Appl. Catal. A: Gen. 170 (1998) 177.
[3] C. Rioche, S. Kulkarni, F.C. Meunier, J.P. Breen, R. Burch, Appl. Catal. B 61 (2005) 130.
[4] A.M. O'Connor, F.C. Meunier, J.R.H. Ross, Stud. Surf. Sci. Catal. 119 (1998) 819.
[5] J. Xu, C.M.Y. Yeung, J. Ni, F. Meunier, N. Acerbi, M. Fowles, S.C. Tsang, Appl. Catal. A 345 (2008) 119.
[6] D. Sutton, B. Kelleher, J.R.H. Ross, Fuel Proc. Technol. 73 (2001) 155.
[7] U. Arena, Waste Manage. 32 (2012) 625.
[8] R. Bain, D. Dayton, D. Carpenter, S. Czernik, C. Feik, R. French, K. Magrini-Bair, S. Phillips, Ind. Eng. Chem. Res. 44 (2005) 7945.

[9] Ø. Borg, N. Hammer, B.C. Enger, R. Myrstad, O.A. Lindvåg, S. Eri, T.H. Skagseth, E. Rytter, J. Catal. 279 (2011) 163.
[10] A. Di Carlo, D. Borello, M. Sisinni, E. Savuto, P. Venturini, E. Bocci, K. Kuramoto, Int. J. Hydrogen Energy 40 (2015) 9088.
[11] K. Sato, K. Fujimoto, Catal. Commun. 8 (2007) 1697.
[12] V.L. Dagle, R. Dagle, L. Kovarik, A. Genc, Y.-G. Wang, M. Bowden, H. Wan, M. Flake, V.-A. Glezakou, D.L. King, R. Rousseau, Appl. Catal. B: Environ. 184 (2016) 142.
[13] D. Mei, V.-A. Glezakou, V. Lebarbier, L. Kovarik, H. Wan, K.O. Albrecht, M. Gerber, R. Rousseau, R.A. Dagle, J. Catal. 316 (2014) 11.
[14] H.S. Bengaard, J.K. Nørskov, J. Sehested, B.S. Clausen, L.P. Nielsen, A.M. Molenbroek, J.R. Rostrup-Nielsen, J. Catal. 209 (2002) 365.
[15] Y. Wang, Y.H. Chin, R.T. Rozmiarek, B.R. Johnson, Y. Gao, J. Watson, A.Y.L. Tonkovich, D.P. Vander Wiel, Catal. Today 98 (2004) 575.
[16] A. Yamaguchi, E. Iglesia, J. Catal. 274 (2010) 52.
[17] M. Luneau, E. Gianotti, F.C. Meunier, C. Mirodatos, E. Puzenat, Y. Schuurman, N. Guilhaume, Appl. Catal. B: Environmental 203 (2017) 289.
[18] J. Sehested, Catal. Today 111 (2006) 103.
[19] J.R. Rostrup-Nielsen, J. Sehested, J.K. Norskov, Adv. Catal. 47 (2002) 65.
[20] C.A. Bernardo, I. Alstrup, J.R. Rostrup-Nielsen, J. Catal. 96 (1985) 517.
[21] F. Josuinkas, C. Quitete, N. Ribeiro, M. Souza, Fuel Process. Technol. 121 (2014) 76.
[22] R. Coll, J. Salvado, X. Farriol, D. Montane, Fuel Process. Technol. 74 (2001) 19.
[23] U. Wolfesberger, I. Aigner, H. Hofbauer, Environ. Prog. Sustain. Energy 28 (2009) 372.
[24] T. Carlson, G. Tompsett, W. Conner, G. Huber, Top. Catal. 52 (2009) 241.
[25] R. Millini, F. Frigerio, G. Bellussi, G. Pazzuconi, C. Perego, P. Pollesel, U. Romano, J. Catal. 217 (2003) 298.
[26] S. Li, T. Boucheron, A. Tuel, D. Farrusseng, F. Meunier, Chem. Commun. 50 (2014) 1824.
[27] S. Li, A. Tuel, D. Laprune, F. Meunier, D. Farrusseng, Chem. Mater. 27 (2015) 276.
[28] D. Farrusseng, A. Tuel, New J. Chem. 40 (2016) 3933.
[29] C. Pagis, A. Morgado Prates, D. Farrusseng, N. Bats, A. Tuel, Chem. Mater. 28 (2016) 5205.
[30] S. Li, A. Tuel, F. Meunier, M. Aouine, D. Farrusseng, J. Catal. 332 (2015) 25.
[31] D. Laprune, A. Tuel, D. Farrusseng, F.C. Meunier, submitted, given as supplementary information.
[32] S. Li, L. Burel, C. Aquino, A. Tuel, F. Morfin, J.-L. Rousset, D. Farrusseng, Chem. Commun. 49 (2013) 8507.
[33] N. Novruzova, A. Tuel, D. Farrusseng, F. Meunier, Microporous Mesoporous Mater. 228 (2016) 147.
[34] S. Li, C. Aquino, L. Gueudré, A. Tuel, Y. Schuurman, D. Farrusseng, ACS Catal. 4 (2014) 4299.
[35] S. Li, A. Tuel, J. Rousset, F. Morfin, M. Aouine, L. Burel, F. Meunier, D. Farrusseng, ChemNanoMat 2 (2016) 534.
[36] ASTM D5758-01, Standard Test Method for Determination of Relative Crystallinity of Zeolite ZSM-5 by X-Ray Diffraction, ASTM, International, West Conshohocken, PA, 2001.
[37] H.G. Merkus, Particle Size Measurements: Fundamentals, Practice, Quality, Springer Ed., 2009, ISBN 978-1-4020-9016-5.
[38] R. Van Hardeveld, F. Hartog, Surf. Sci. 15 (1969) 189.
[39] J. Wei, E. Iglesia, J. Catal. 224 (2004) 370.
[40] C.H. Bartholomew, R.B. Pannell, J. Catal. 65 (1980) 390.
[41] J.P. Candy, A. Elmansour, O.A. Ferretti, G. Mabilon, J.P. Bournonville, J.M. Basset, G. Martino, J. Catal. 112 (1988) 201.
[42] H. Liu, Ammonia Synthesis Catalysts: Innovation and Practice, 7, World Scientific Publishing, 2013, pp. 586.
[43] M. van der Meijden, P.C.A. Bergman, A. van der Drift, B.J. Vreugdenhil, Preparations for a 10 MWth bio-CHP, in: 18th European Biomass Conference and Exhibition, Lyon, France, 2010, pp. 3–7.
[44] http://eurokin.tudelft.nl/.
[45] S.P. Zhdanov, N.N. Feoktistova, N.I. Kozlova, I.G. Polyakova, Bull. Acad. Sci. USSR Div. Chem. Sci. 34 (1985) 2467.
[46] M.C.J. Bradford, M.A. Vannice, Appl. Catal. A 142 (1996) 73.
[47] H.M. Swaan, V.C.H. Kroll, G.A. Martin, C. Mirodatos, Catal. Today 21 (1994) 571.
[48] D.L. Trimm, Catal. Today 49 (1999) 3.
[49] J. Jae, G.A. Tompsett, A.J. Foster, K.D. Hammond, S.M. Auerbach, R.F. Lobo, G.W. Huber, J. Catal. 279 (2011) 257.